A methodology for online characterization of the deconsolidation of fiber-reinforced thermoplastic composite laminates

Luc Amedewovo [a], Arthur Levy [a,*], Basile de Parscau du Plessix [a], Julien Aubril [a], Arnaud Arrive [a], Laurent Orgéas [b], Steven Le Corre [a]

[a] *Nantes Université, IRT Jules Verne, CNRS, Laboratoire de Thermique Et énergie de Nantes, LTeN, UMR 6607, F-44000 Nantes, France*
[b] *Univ. Grenoble Alpes, CNRS, Grenoble INP, 3SR Lab, 38000 Grenoble, France*

ARTICLE INFO

ABSTRACT

Pre-consolidated fiber-reinforced thermoplastic laminates often need a secondary manufacturing step such as welding, forming. When a low pressure is applied during the laminate heating stage, porosities can appear in various forms (bubbles, delaminations, *etc.*). This is the deconsolidation phenomenon. These porosities significantly deteriorate the mechanical properties of the composites. Usually, deconsolidation is characterized by analysis after processing or by Thermomechanical Analysis (TMA). However, these techniques do not allow online investigation of deconsolidation mechanisms on representative composite laminates.

In order to overcome these limitations, a new experimental device has been developed. It allows the online characterization of fiber-reinforced thermoplastic laminate deconsolidation, by continuous measurement of deconsolidation strain of samples with large size (several centimeters in contrast to a few millimeters in TMA) under representative heating conditions. The capability of the setup is illustrated on plate samples made of a high-performance Carbon Fiber (CF) - reinforced thermoplastic (CF/PEKK laminates).

1. Introduction

The demand for composite materials in the aeronautical sector is continuously growing, due to their high specific mechanical properties. Thermoset Carbon Fiber-reinforced Polymers (CFRPs) which are commonly used in aeronautics, present major issues mainly related to assembly [1–3]. One of the solutions to avoid this problem is the use of thermoplastic CFRPs.

Unlike thermoset matrix CFRPs, thermoplastic matrix CFRPs can be repeatedly reheated and then re-consolidated, reformed as well as welded. However, when a low or no pressure is applied during heating, porosities appear and may remain in the final part after processing: this is the deconsolidation phenomenon. It is well known that porosities strongly degrade the mechanical strength of materials [4–6]. It is, therefore, crucial to avoid deconsolidation during processing. For that purpose, the mechanisms involved during deconsolidation of fiber-reinforced thermoplastic composites must be properly characterized and understood.

Many studies in the literature showed that deconsolidation of thermoset composites laminates, during curing, is mainly due to volatile diffusion mechanisms [7–9]. In fact, volatile substances are trapped in the material during its storage in a freezer or during its lay-up in a room environment. Under temperature and pressure effect, the volatiles cause deconsolidation through diffusion mechanisms. Based on these results, some authors suggest that thermoplastic composite deconsolidation could also be related to the same mechanisms. To verify this hypothesis, most of the work in the literature has focused on glass fiber-reinforced thermoplastic composites [10–12]. Recently Slange et al. [13] carried out deconsolidation tests (in an convection oven) on dried and undried UniDirectional (UD) $[0/90]_{4s}$ Carbon Fiber/PolyEtherEtherKetone (CF/PEEK) laminate samples, consolidated at 1 MPa in a press. The results showed that the thickness increase of dried samples after deconsolidation is smaller than undried ones. Slange et al. then concluded that moisture diffusion is the main factor responsible for deconsolidation in press consolidated UD CF/PEEK laminates samples. Consequently, the authors recommended drying the laminates at 250 °C for 3 h, in order to eliminate moisture effects before laminates processing.

Unlike thermoset composites, synthetic and oil-based thermoplastic composites (TPC) usually absorb less moisture than thermoset composites. For this reason, other authors showed that the deconsolidation of these hydrophobic thermoplastic laminates is mainly caused by relaxation of residual stresses stored in the laminates after their consolidation. In the literature, this hypothesis is mainly highlighted for

woven and mat laminates [14–16]. To our knowledge, in the case of high performance UD TPC laminates, only Donadei et al. [17], showed that deconsolidation is linked to stress relaxation. To do so, the authors carried out deconsolidation tests (in an infrared oven) on annealed and non-annealed UD $[-45/90/45/0]_{3S}$ CF/PolyEtherKetoneKetone (PEKK) laminates consolidated at 0.6 MPa in an autoclave.

These different conclusions suggest that both moisture and residual stress may be involved in the deconsolidation phenomenon. It also appears as difficult to decorrelate these two effects. Indeed, drying and relaxing residual stresses are usually performed altogether during preconditioning.

In most of the studies performed, deconsolidation is characterized by analysis after experiment (thickness measurement, micrographs, *etc.*) [13,17,18]. These characterization methods do not allow the analysis of what happens during heating and dwell. Indeed, during cooling, shrinkage and crystallization phenomena can affect the final state (thickness) of the material. It is then difficult with these techniques to characterize the real impact of the consolidation processes and the volatile substances initially stored in the material on deconsolidation.

Another solution mainly used to characterize deconsolidation during heating is Thermomechanical Analysis (TMA) [19]. It allows the application of representative cycles to a small lab scale sample (8 mm × 8 mm). However, deconsolidation may be affected by free stress edges, if the sample size is not representative of a laminate structure. Brzeski [20] uses image correlation method to characterize deconsolidation of 50 mm × 50 mm woven laminates made of glass fiber-reinforced plastics. The team measured online thickness evolution due to deconsolidation in a press, using CCD camera. Unfortunately, they did not analyze the measurements. This is probably because of the edge effect, as the thickness was measured on the lateral side of the sample. Deconsolidation, indeed, mostly occur in the core [12,13,17]. Furthermore, no information was mentioned on the validation of the measurements and a thermal analysis was not performed to estimate the samples temperature field during the experiments.

The major contribution of this work is the design, fabrication and validation of a new device. It can characterize continuously and online deconsolidation of high-performance fiber-reinforced thermoplastic composite. This device will allow online observation of the phenomena involved during heating, on samples of sizes representative of a structure. This is illustrated with a aerospace grade TPC laminates CF/PEKK initially consolidated by Hot Press consolidation and deconsolidated under various conditions. These test results enabled preliminary understanding of the effect of moisture and residual stresses on subsequent TPC laminate deconsolidation.

2. Continuous and online COmposite DEconsolidation Characterization bench (CODEC)

CODEC bench is developed for continuous and online characterization of large TPC laminates deconsolidation under different processing conditions (pressure, temperature, heating rate, *etc.*). Deconsolidation is characterized on the device by a thickness variation measurement using optical sensors. The thickness variation measured correspond to the macroscopic structural change in the material due to porosities appearance and growth (deconsolidation).

2.1. Development

The device is composed of a large copper heating plate which can heat up to 450 °C with a maximal heating rate of 60 °C/min (Fig. 1). The hot plate temperature is measured by a K-type monitoring thermocouple sensor located in the middle of the hot plate, 1 mm beneath its surface. The heating power is generated by resistive cartridge heaters and regulated according to the temperature measured by the monitoring thermocouple. The hot plate is placed in a closed thermal chamber (aluminum) with a 25 mm thick borosilicate upper

glass window. In order to limit the thermal chamber expansion due to temperature variations, the chamber walls are cooled by an active water flow in the sole. Two Pamitherm thermal insulators are placed between the sole and the hot plate to reduce conductive heat transfer between the hot plate and the aluminum chamber. The chamber is equipped with a compressed gas inlet, to pressurize the chamber up to 1 MPa (10 bars). The sample can also be processed in a classical vacuum bag setup and a gas-tight passage permits the sample to be vacuumed. During experiments on CODEC device, the sample can be let free under atmospheric pressure, in the thermal chamber. This case refers to a test at no counter pressure. When a vacuum pressure (0.1 MPa) is required for a test, the sample is surrounded by edging frames, acting as dams, and placed under a vacuum bag (Fig. 1a). A primary vacuum (≈0.01 MPa) is then applied under the vacuum bag through a VARIAN SD-450 serial no. 241687 vacuum pump connected to the gas-tight passage. It should be noted that only the sample is under vacuum and the thermal chamber is still at an atmospheric pressure. Finally, the sample can be processed as in an autoclave. In addition to the vacuum pressure in the bag, an inert gas can be injected in the thermal chamber to increase the counter pressure, up to a given absolute value. The chamber pressure is measured by a pressure sensor, from Keller's 35XTC series. The chamber is designed for a pressure of up to 1 MPa. The pressure sensor has a larger measurement range of 0 to 3 MPa and an accuracy of ±0.05% of the measurement range. The chamber is also equipped with a safety valve to evacuate the gas in case of overpressure.

The samples thickness variation is measured using 3 Keyence IL-S065 laser sensors through the borosilicate window. The three distance measurement sensors have a measurement range of 55 to 75 mm and a linearity of ±0.075% of the full scale. The laser emitted by the sensors has a wavelength of 655 nm (visible light), to which the borosilicate is transparent. The maximum environmental temperature that the sensors can withstand is 50 °C. For this reason, the sensors are positioned in an aluminum box located on a structure outside the chamber. This solution is however insufficient to protect the sensors, given the radiation emitted by the hot plate which passes through the glass window. A 3 mm thick aluminum barrier plate is thus placed between the hot plate and the glass window. The barrier plate mainly plays 2 roles. The first role is to avoid a significant rise of the glass window temperature, by reflecting and absorbing the heat emitted by the hot plate. The emissivity of the barrier plate is minimized by polishing its faces. This barrier also helps to avoid significant distortion of the glass window, which can lead to significant measurement errors of the laser sensors. The second role of the barrier plate is to limit gas convection movements in the chamber, which cause significant noise on the sensors measurement. The holes machined in the barrier plate for the laser rays passage are covered by 2 mm thick borosilicate glass plates.

Laser and pressure sensors, thermocouples, and power controller are connected by means of modules to a single NI CompactDAQ acquisition system. The control is performed automatically using a single piece of software developed on labVIEW. Thus, the temperature, pressure, distance data acquisition, and temperature control are synchronized. This provide a better control of the experiment conditions (heating rate, temperature, pressure).

2.2. Thickness variation measurement

Among the three laser sensors placed on the CODEC device, only two sensors aim at the sample. The first sensor (S1) aims at the hot plate (Fig. 2 left). The second sensor (S2) aims at the center of the sample and the last one (S3) aims 40 mm from the center. During a ramp-up, the distances between the sensor positions and the targets (sample and hot plate) are recorded (Fig. 2 right). From the distance measurements, elongations (expansion or contraction of the targets) are obtained at the three measurement points, as the difference between the actual distance and the initial ones as depicted in Eq. (1). The hot plate elongation
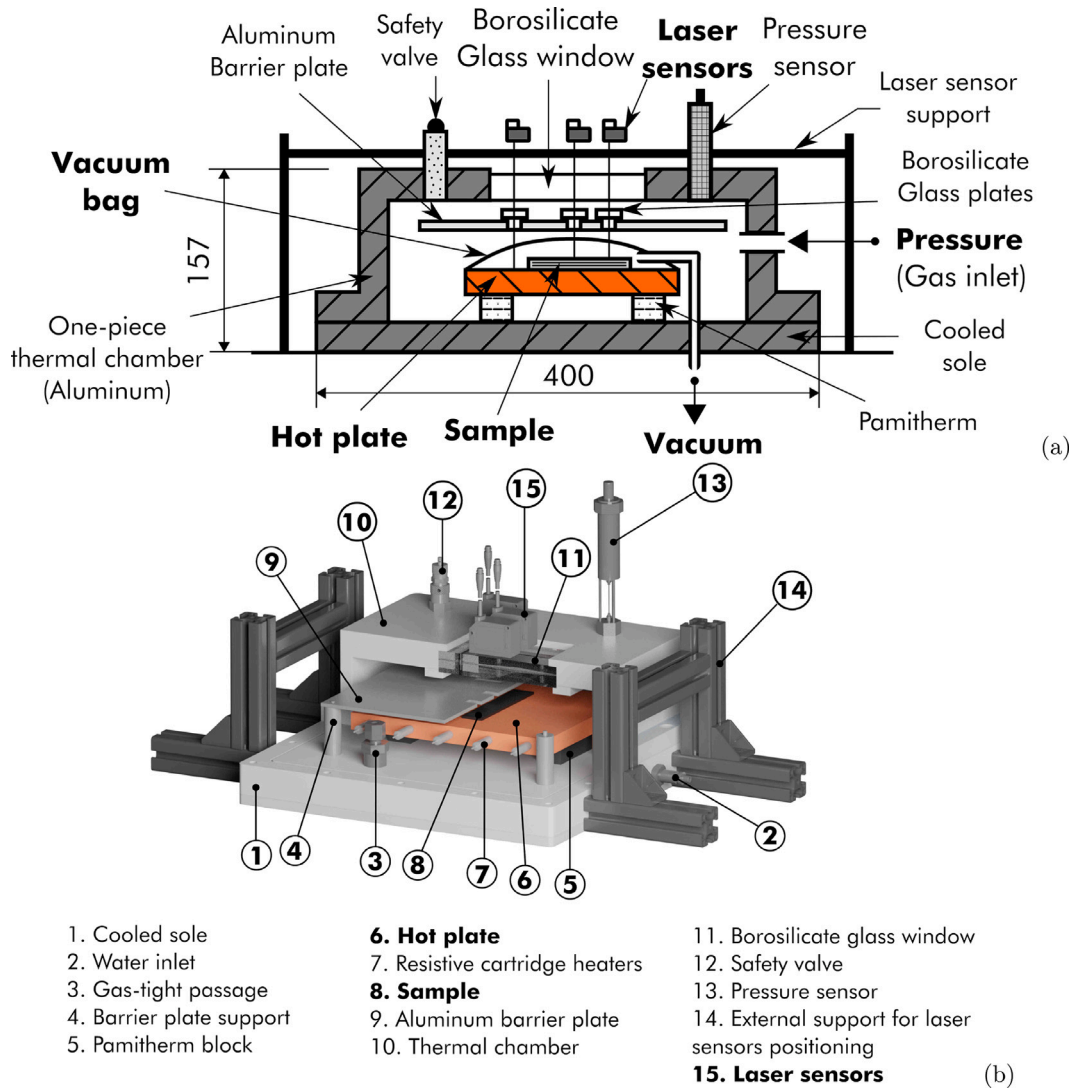
Fig. 1. CODEC bench designed for continuous and online characterization of thermoplastic composite laminates deconsolidation under processing conditions. Laminate thickness evolution is measured in the chamber with contactless laser sensors. (a) CODEC schematic view and (b) CAD view.

(baseline, S1) was subtracted from the total elongation calculated on the sample (2). This procedure allowed us to estimate the real sample elongation.

$$\Delta L_i(t) = D_i(0) - D_i(t) \quad i = \{S1; S2; S3\} \tag{1}$$

$$\Delta L_j(t) = \Delta L_j(t) - \Delta L_{S1}(t) \quad j = \{S2; S3\} \tag{2}$$

$$\varepsilon_D = \varepsilon_j(t) = \ln\left(1 + \frac{\Delta L_j(t)}{L_0}\right) \tag{3}$$

where $D_i(0)$ is the initial distance measured at a given measurement point, $D_i(t)$ the distance over time, $\Delta L_j(t)$ and ε_j respectively the sample elongation and strain at the two measurement points, L_0 is the sample initial thickness measured by a micrometer.

The sample deconsolidation true strain (ε_D) was then determined according to Eq. (3) at the two measurement points. This deconsolidation strain is a global strain. Indeed, the strain is heterogeneous during TPC laminates deconsolidation. Hencky or logarithmic strain is used because of the high strains produced by deconsolidation. Distance, temperature, and pressure measurements are synchronized on CODEC device. It is thus possible to characterize the deconsolidation of large samples (up to 150 mm × 50 mm), under controlled conditions of temperature and pressure representative of industrial processes (autoclave, VBO, etc.).

2.2.1. Measurement validation

In order to estimate the accuracy of the developed CODEC bench, the setup was tested with a reference homogeneous metallic sample, *i.e.*, 6061 aluminum. The metallic sample does not experience phase change or deconsolidation during heating in the tested temperature range. The expansions measured with the CODEC bench are compared with standard dilatometry measurement.

Firstly, using a Linseis L75HS500LT dilatometer, the dilatometry test was performed on a 10 mm × 10 mm × 2.98 mm sample of 6061 aluminum. The sample was heated at 2 °C/min from 20 °C to 300 °C. Strain as a function of temperature is plotted on Fig. 3. From this curve, the linear CTE was determined along the thickness direction (Table 1).

Secondly, using the CODEC bench, another test was performed on a bigger plate (125 mm × 25 mm × 2.98 mm) of the same alloy. The size of the sample was increased in order to avoid edge effects related to air convection, according to the hot plate size and the thermal chamber volume. The sample was heated at 5 °C/min up to 300 °C under a vacuum pressure (0.1 MPa). This dilatometry test was repeated twice. Since aluminum has a high thermal conductivity ($\approx$167 W m^{-1} K^{-1}), the defined heating rate allowed to obtain an homogeneous temperature in the aluminum sample. During the test, one K-type thermocouple
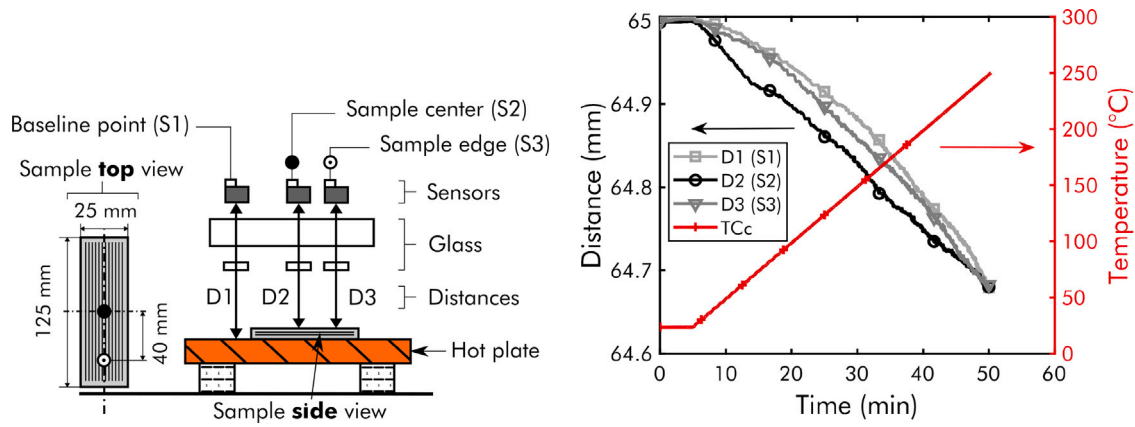
Fig. 2. Validation of the CODEC bench using an aluminum sample. (left) positioning of the contactless laser sensors (right) example of raw distance measurement vs time during a ramp up of 5 °C/min up to 250 °C on an aluminum sample.
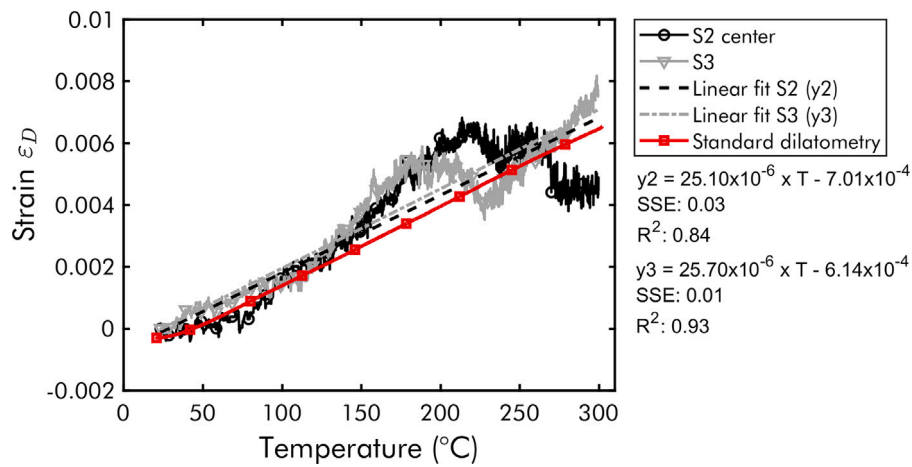

Fig. 3. Comparison between dilatometry test results obtained by standard dilatometer and by CODEC device, on an aluminum sample. On CODEC device, vacuum pressure is applied on the sample.

Table 1
Comparison of CTEs obtained by standard dilatometry and with the CODEC bench.

Dilatometry (°C⁻¹)	25.67×10^{-6}	
Codec setup (°C⁻¹)	Sensor 2	Sensor 3
Test 1	25.10×10^{-6}	25.70×10^{-6}
Test 2	25.57×10^{-6}	24.65×10^{-6}
Mean	25.34×10^{-6}	25.18×10^{-6}
Absolute error (°C⁻¹)	0.33×10^{-6}	0.49×10^{-6}
Relative error (%)	1.29	1.91

was placed on the top surface of the sample (TC5) and another directly taped on the copper top surface below the vacuum bag (TCs). The maximum temperature difference between the two measurements was 4 °C (Fig. 4). TC5 thermocouple is pressed against the aluminum top surface by the vacuum bag. Thus, the measured temperature at this point is assumed to be the aluminum sample temperature. The vacuum pressure is applied during the experiment in order to maintain a good contact between the sample and the hot plate. The sample strain as a function of temperature is plotted on Fig. 3.

2.2.2. Accuracy of the CODEC setup

The strain curve obtained with the CODEC device is rather non-linear and scattered (Fig. 3). This non-linearity is due to the macroscopic movements of the heating plate on its Pamitherm blocks (Fig. 1) and the air convection which disturbed the laser measurement. Indeed,
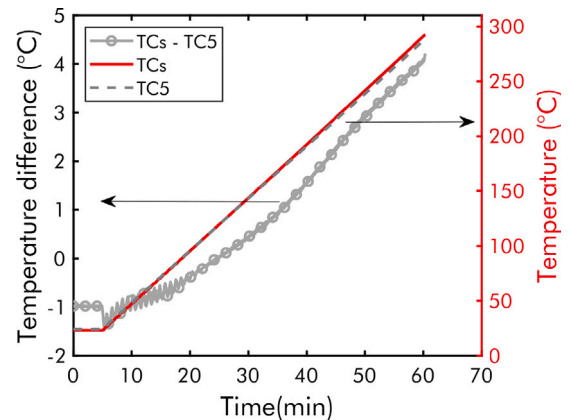

Fig. 4. Temperature difference between the top surface temperature of the aluminum sample (TC5) and the top surface temperature of the hot plate (TCs).

the distance measurement is based on laser triangulation principle. For this reason, the measurement is affected by the environment conditions (air convection and temperature) and the hot plate flatness.

Moreover, the measure strain deviates above 150 °C. It is assumed that this is probably due to an optical effect related to the aluminum sample. This deviation was not repeatable and was not observed on composite samples tests (see Section 4.2). Furthermore, the magnitude

Fig. 5. Micrograph of the consolidated samples before deconsolidation tests. The initial porosity content is not measurable.

of this deviation is small (0.2% strain) and negligible compared to the strains in composite samples ($\gg$5%) during deconsolidation.

A comparison of the CTEs obtained, with a standard dilatometer and with the CODEC device, was performed at the measurement points (Table 1). These CTEs were obtained by a linear regression over a temperature range of 25 °C to 300 °C. The CTEs comparison shows that the CODEC device is able to characterize small strains with a relative error of $\pm 2\%$. As it will be clear in the following, such a precision enables to properly observe and quantify the targeted phenomena.

3. Material and procedure

In order to investigate the deconsolidation phenomenon occurring on an aerospace grade thermoplastic composite material, UD CF/PEKK composite laminates were tested with the CODEC bench.

3.1. Carbon/PEKK composite manufacturing

The CF/PEKK prepreg plies were supplied by Toray Advanced Composite. The plies have a fiber areal weight (FAW) of 194 g m^{-2} and a theoretical thickness of 0.185 mm. The resin mass content is 34 %. The glass transition temperature (Tg) and melting temperature (Tm) of PEKK 7002 are 160 °C and 337 °C, respectively (according to the manufacturer). In practice, the melting zone observed during DSC experiments extends between 310 °C and 360 °C, with a melting peak at 338 °C. This melting range can also be found in [21–23].

From the prepreg plies, $[0]_{16}$ laminates were consolidated in a hot press. The 348 mm × 348 mm prepreg plies were stacked in a picture-frame mold (internal cavity dimensions: 350 mm × 350 mm) and consolidated on a 50 t Pinette P.E.I press according to the following cycle : heating at 10 °C/min up to 380 °C under a pressure of 0.1 MPa; the temperature was held for 20 min under a pressure of 4 MPa; cooling at 10 °C/min at the same pressure, then demolding. The final part dimensions after consolidation are 350 mm × 350 mm × 2.90 mm. This final size of the laminate is due to the high pressure and the clearance between the plies and the internal cavity of the mold which promotes PEKK resin squeeze out.

Optical micrographs of the consolidated laminates validate a porosity content lower than the measurement limit after the consolidation (Fig. 5). To perform the microscopic observations, 25 mm wide samples were encapsulated using a slow-curing epoxy resin (EpoFix, Struers). The samples were then prepared using traditional grinding and polishing techniques on an automated polishing machine (Tegrapol-21 and TegraForce-5, Struers) and observed on the digital microscope KEYENCE VHX-7000 series. The cross section micrographs were obtained by assembling several sections with a resolution of 2880 px × 2160 px resulting in an image with a large area of observation and a good resolution. Using the trainable weka segmentation algorithm [24] in an image processing software (Fiji), the porosity content was measured.

This microscopic observation was validated by a micro-CT analysis which showed an initial porosity content of 0.02% (Fig. 6). This value is a minor of the laminate porosity content. The 3D image of the sample (20 mm diameter) was obtained on one of the X-ray tomographs of the ID19 line at European Synchrotron Radiation Facilities (Grenoble, France). The raw 3D image was produced (i) with a voxel size of 3.81^3 μm^3 and a large observation area (2016 × 2016 × 1410 pixels), (ii) by

Table 2
CF/PEKK $[0]_{16}$ laminate thermal properties.

	Density ρ (kg m^{-3})	Specific heat capacity C_p (J kg^{-1} K^{-1})
$T < T_g$	$\rho(T) = 1602.7 - 0.10 \times T \ [°C]$	$C_p(T) = 2.62 \times T \ [°C] + 769.7$
$T > T_g$	$\rho(T) = 1605.8 - 0.40 \times T \ [°C]$	$C_p(T) = 2.34 \times T \ [°C] + 850.6$
$T > 300 \ °C$		$C_p(T) = 0.75 \times T \ [°C] + 1296$
	Transverse conductivity k_z (W m^{-1} K^{-1})	
$T < T_g$	$k_z(T) = 8.76 \times 10^{-4} \times T \ [°C] + 0.73$	
$T > T_g$	$k_z(T) = 7.31 \times 10^{-4} \times T \ [°C] + 0.81$	

using Paganin method [25]. Additional post-treatment on a Region Of Interest (ROI) of 1000 × 1000 × 650 pixels (picked from the raw 3D image) using the trainable weka segmentation algorithm, in an image processing software (Fiji), allowed to measure the porosity content.

3.2. Thermal characterization

The thermal properties of the consolidated laminate are given in Table 2. These data were obtained, following the procedure detailed by Avenet [22]. The thermal characterization (DSC, guarded hot plate, hydrostatic weighing, and TMA) was performed on samples taken from hot press consolidated laminates. Note that the carbon fibers used by Avenet are different from the ones used in this study.

The material heat capacity was obtained, using a TA Instruments DSC Q200. The measurement was performed on a 53.8 mg composite laminate sample of 4 mm diameter cut, by waterjet. The sample was first heated at 20 °C/min up to 400 °C/min in order to erase its thermal history related to the consolidation process. The heat capacity measurement was then performed during a second heating of the sample at 5 °C/min up to 400 °C. The same cycle was applied on an empty specimen holder to obtain the baseline for the heat capacity determination. The low heating rate during the experiments allowed to minimize thermal gradients in the sample during the measurements.

The material thermal conductivity was obtained by standard guarded hot plate method (according to standard ISO 8302:1991) on a sample of 15 mm × 15 mm surrounded by a guard cut from the same laminate (CF/PEKK). The thermal conductivity measurements were performed at different temperatures between 25 °C and 245 °C. The linear relation between the temperature and the thermal conductivity was obtained by a linear fit of the experimental data. Further details about the equipment used to obtained the thermal conductivity can be founded in [22,26]. The hydrostatic weighing was performed on five composite samples of 20 mm diameter, using a METTLER TOLEDO AG245 balance with 10 μg accuracy. The reference liquid used was ethanol. Finally, the TMA measurements were performed on a Linseis L75HS500LT dilatometer where the sample were heated at 2 °C/min up to 300 °C.

3.3. Preconditioning

After consolidation, the large laminates were cut into small 125 mm × 25 mm samples using a Protomax waterjet cutting machine. The samples were then separated into two groups: Dried Samples (DS) and Ambient Storge (AS) samples.
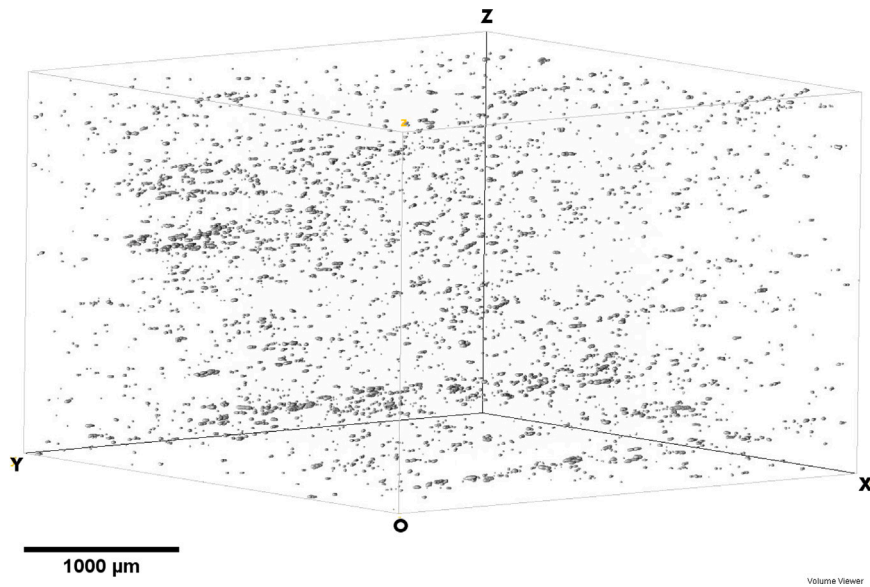
Fig. 6. 3D image of the porosity distribution in a sample of 20 mm diameter cut from the consolidated laminate (Region Of Interest size: 1000 × 1000 × 650 pixels). The porosity content is 0.02%.

The DS samples were dried at 180 °C for 72 h in order to eliminate residual moisture. This drying condition was carefully checked by continuous weight measurement during drying tests at different temperatures (140 °C, 180 °C, 250 °C), using an OHAUS Explorer EX125M balance with an accuracy of 10 μg. Drying at 180 °C for 72 h fully eliminated the effect of humidity without any thermal degradation of the material (no further significant weight change was observed at 180 °C over this duration of drying).

The AS samples were stored in the workshop for 5 months in ambient condition. After a drying test on a 80 mm × 80 mm AS sample at 180 °C, a weight measurement showed that the water content of the stored samples is 0.013% at the end of the storage. Both groups of samples allow us to investigate the effect of moisture and residual stresses on deconsolidation.

3.4. Deconsolidation tests

Thereafter, the 125 mm × 25 mm samples were deconsolidated within the CODEC setup. The samples were heated at 60 °C/min or 10 °C/min up to 380 °C, then maintained at this temperature for 5 min, and cooled (natural convection between the sample and air). The test matrix is shown in Table 3. This heating cycle is representative of a typical temperature cycle for CF/PEKK during its processing. During the heating, the sample can be let free under atmospheric pressure in the thermal chamber. This is the case of the test at no counter pressure where no vacuum and no external pressure was applied.

The last test was performed on a DS sample at 0.5 MPa. In this latter case, not only the sample is maintained under vacuum in the bag, an inert gas is injected in the thermal chamber to increase the counter pressure up to an absolute value of 0.5 MPa. This pressure value is half of the maximum pressure that can be reached with the CODEC bench in the thermal chamber. It is representative of autoclave processing.

3.5. Composite sample temperature estimation

During the non-isothermal deconsolidation test, the temperature measured by the thermocouple implemented in the hot plate is not representative of the composite sample temperature. In particular, this is due to the non perfect plate/sample contact inducing thermal contact resistance. For a proper analysis of the thermomechanical conditions of
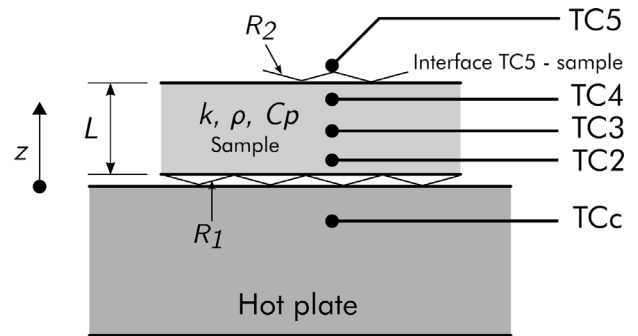

Fig. 7. Estimation of the effective laminate temperature using a through thickness heat transfer model. The model is fitted using 5 thermocouple measurements. R_1 and R_2 represent the thermal conductances between (i) the copper and composite lower face and (ii) the composite upper face and taped thermocouple TC5.

Table 3
Deconsolidation tests.

Test #	Conditioning	Counter pressure	Heating rate	Repeat
1	AS	No counter pressure	60 °C/min	3
2	DS	No counter pressure	60 °C/min	3
3	AS	No counter pressure	10 °C/min	3
4	DS	No counter pressure	10 °C/min	3
5	DS	0.5 MPa	10 °C/min	1

the deconsolidation occurrence, the temperature inside the composite sample has to be estimated more accurately. In this section, heat transfer is modeled to estimate the temperature distribution in the composite part using an AS sample instrumented with three embedded thermocouples (Fig. 7). One thermocouple is located at the sample center (TC3) and the others two plies deep (≈0.4 mm) underneath the sample upper (TC4) and lower face (TC2).

3.5.1. Modeling
Because of the aspect ratio of the samples (125 mm × 25 mm × 2.90 mm), the heat transfer in the composite plate was modeled using a one dimensional heat equation through its thickness L, ie:

$$\rho(T)C_p(T)\frac{\partial T}{\partial t} = \frac{\partial}{\partial z}\left(k_z(T)\frac{\partial T}{\partial z}\right) \quad \forall z \in [0, L] \tag{4}$$
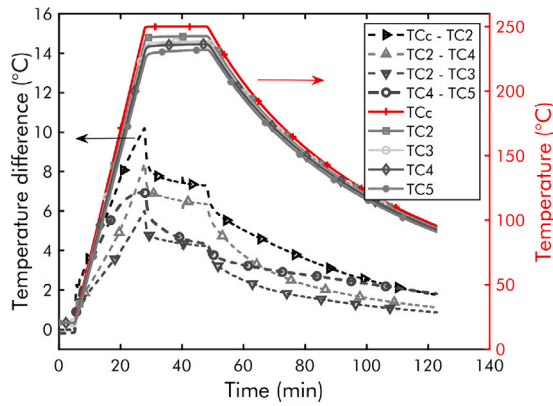
Fig. 8. TC measurements at a heating rate of 10 °C/min and no applied counter pressure.

where ρ is the composite density, C_p its heat capacity and k_z its through thickness or transverse conductivity. These properties are given in Table 2 in Section 3.2. Mixed boundary conditions are considered at both surfaces of the composite plate:

- At the contact with the copper platen, the heat flux writes:

$$k_z \frac{\partial T}{\partial z}(z = 0, t) = -\frac{TCc - T}{R_1} \qquad (5)$$

where R_1 accounts for the thermal contact resistance between the sample and the copper platen and TCc is the copper platen temperature which is considered uniform and known as measured by the thermocouple (Fig. 7).

- At the upper surface, the heat flux writes:

$$k_z \frac{\partial T}{\partial z}(z = L, t) = \frac{TC5 - T}{R_2} \qquad (6)$$

where R_2 is the thermal contact resistance between the taped thermocouple and the sample upper face. TC5 is measured with the taped upper thermocouple (Fig. 7). The measured temperature at TC5 accounts for both the conducto-convective exchange with the air and the radiative exchange with the facing barrier plate.

For a given set of constant R_1 and R_2 thermal resistances, the above transient one dimensional heat transfer model was solved. Spatial integration used quadratic finite elements and time was integrated implicitly with the backward Euler method. The implementation was done in COMSOL Multiphysics [27].

3.5.2. Boundary conditions identification

A standard inverse method was used to identify the thermal resistance R_1 and R_2 used in Eqs. (5) and (6). The residual consists of the modeled and measured temperature differences for each of the three embedded thermocouples (Fig. 7) at each time step over a temperature cycle at 10 °C/min up to 250 °C, and a dwell of 20 min followed by a natural convection cooling. The residual 2-norm was minimized using the simplex method built in MATLAB [28]. It corresponds to a least squares fit.

Fig. 8 shows the temperature measurements when no pressure is applied on the sample. A significant temperature difference can be observed between the copper and the first thermocouple TC2 near the composite lower surface. Similarly, a temperature gap is observed between the upper face temperature measured by the taped thermocouple TC5 and the last thermocouple TC4 near the composite upper face. These temperature differences are due to the thermal contact resistance at the copper-composite and upper thermocouple-composite interfaces modeled with R_1 and R_2.

Table 4
Thermal resistances in m^2 K W^{-1} identified by inverse method for different pressures.

	No counter pressure	P = 0.1 MPa	P = 0.5 MPa
R_1	16.04×10^{-4}	11.89×10^{-4}	14.24×10^{-4}
R_2	39.48×10^{-4}	12.04×10^{-4}	12.12×10^{-4}

When a vacuum (P = 0.1 MPa) is applied to the composite, a decrease of these temperature differences is observed (Fig. 9). Indeed, the application of pressure improves the contact at the composite's boundaries which leads to a decrease of the thermal resistance at the boundaries. However, when in addition to the vacuum, an overpressure is applied to the sample using pressurized gas (Argon in this case), the temperature differences at the composite boundaries are slightly higher than when only the vacuum is applied (Fig. 9). As pressure improves the contact at the interfaces, the increase in pressure should lead to smaller temperature differences. The opposite trend observed on the CODEC device is due to the continuous pressure regulation. In fact, in order to regulate the pressure in the chamber at the set value, pressurized gas at low temperature ($\approx$20 °C–30 °C) is sent continuously, even during the dwell, to compensate the fluctuations linked to the leaks and the gas thermal expansion in the chamber. The continuous cold gas injection creates a convection flow in the chamber which dissipates a part of the heat emitted by the hot plate and slightly cools the upper part of the composite. This effect was not observed when only vacuum is applied because there is no need for pressure regulation.

In order to reproduce the composite real thermal conditions with the thermal model, the thermal resistances were identified for three different pressures (no counter pressure, 0.1 MPa, 0.5 MPa).

3.5.3. Thermal model validation

The obtained values of thermal resistances are given in Table 4 and the temperature residuals at the sample lower face (Tc2) are plotted versus time in Fig. 10. The maximum difference obtained between the experimental and the computed temperatures at the three measurement points and for the three pressures is 3 °C. The range of the error is therefore ±3 °C. The thermal model developed in this section will allow the estimation of the composite laminate temperature during the deconsolidation tests on the CODEC device.

4. Results and analysis

The results of the deconsolidation tests performed on the CODEC device (listed in Table 3) are presented in this section.

4.1. After experiment analysis

At the end of the deconsolidation tests, mean deconsolidation strain was calculated by thickness measurements at five measurement points on the sample with a micrometer of 0.01 mm accuracy. One point is located on the sample center and the others are spaced 20 mm on each side of the center. In this case the deconsolidation strain ε_D^f after experiment is calculated, at each point, as (7).

$$\varepsilon_D^f = \ln\left(\frac{L_f}{L_0}\right) \qquad (7)$$

where L_f is the final sample thickness after the deconsolidation test, and L_0 the sample initial thickness before the test. Fig. 11 (left) shows the mean ε_D^f of the three repetitions performed for each test condition. The error bar indicates the standard deviation. The low ε_D^f obtained after the test under 0.5 MPa shows that there was no deconsolidation. The difference between the AS and DS samples is also small for both heating rates. From these observations, it can thus be stated that moisture has a negligible impact on deconsolidation and there is no significant effect of heating rate on deconsolidation.
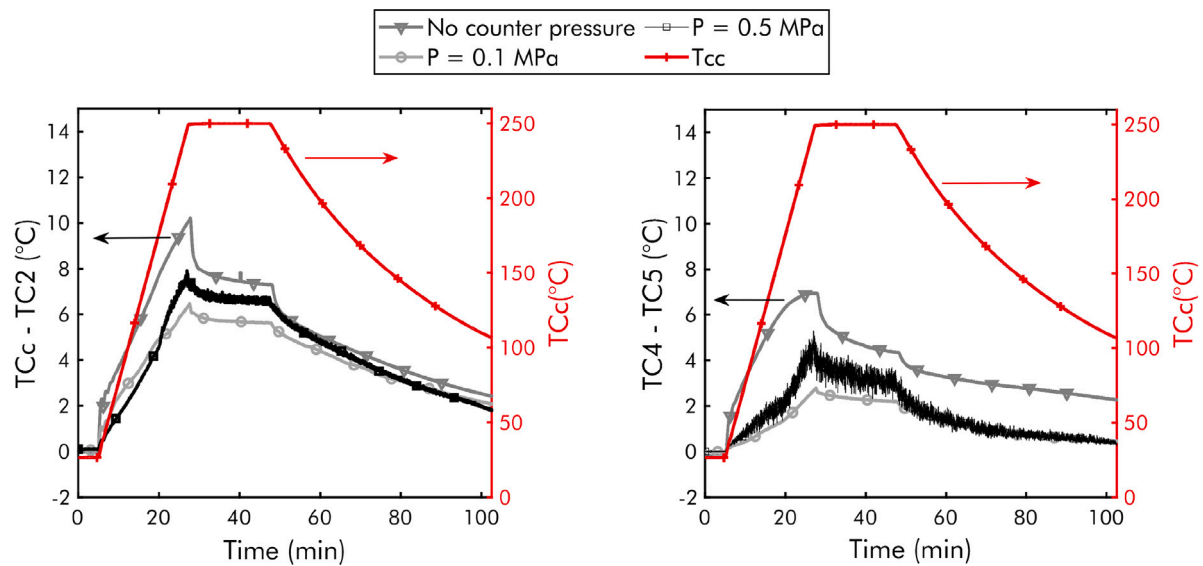
Fig. 9. Effect of pressure on thermal boundary conditions. Temperature discontinuity across (left) the sample lower face and (right) upper face.
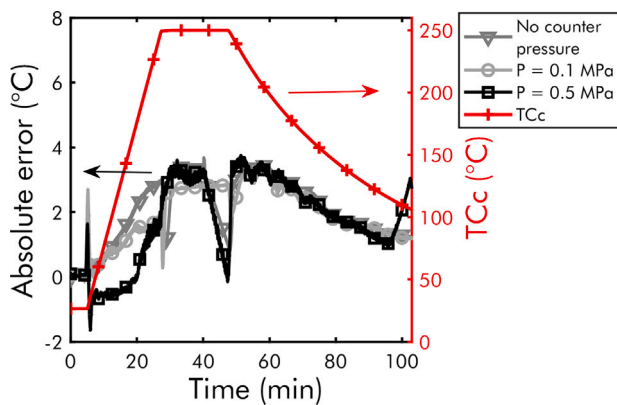

Fig. 10. Model validation at a different pressures.

In order to observe the microstructural changes that result from deconsolidation, micrographs were performed at the end of the deconsolidation tests according to the procedure describe in Section 3.1. The porosity content estimation were performed on three sections per sample. The sections were cut exactly at the same location on all the samples in order to performed a comparative analysis of the porosities distribution and morphology.

Initially, the porosity content of the samples is lower than the measurement limit (Fig. 5). A non measurable porosity content was also observed on the sample tested at 0.5 MPa (Fig. 12e). The highest porosity content was obtained on the AS samples (Fig. 12c). The porosities are also much larger and mainly located at the subsurface. In the DS samples, the porosities have small sizes and are homogeneously located in the middle of the sample (Fig. 12b&d). Moreover, there is a huge difference (8 %) between the porosity content of AS and DS samples at 10 °C/min (Fig. 11 right). This difference may be related to the lack of sufficient number of micrographs per sample. Nevertheless, the pore morphology and distribution clearly shows a significant effect of moisture and heating rate on deconsolidation. However, the final measured thickness indicates a small strain difference ($\Delta\varepsilon_D^f = 0.02$) between the AS and DS sample (see Fig. 11 left). The micrographs thus show that the differences in the samples microstructure cannot be highlighted with only deconsolidation strains measured after experiment. In order to explain these microstructure differences, continuous and online characterization of the deconsolidation is required. The results obtained by the online measurement are subsequently analyzed to better understand the mechanisms involved during the deconsolidation experiments.

4.2. Online measurements analysis

On the CODEC device, three data are obtained after each deconsolidation test (Fig. 13 left): the hot plate temperature; the sample upper face temperature and the sample deconsolidation strain, at the two measurement points calculated from the distance measurements.

According to the unilateral heating, we can expected that deconsolidation will start at the samples lower face. In order to estimate the samples lower face temperature, the measured temperatures TCc and TC5 are used as boundary condition in the thermal model developed in Section 3.5. The lower face temperature is estimated as the average of the simulated temperature field over a thickness corresponding to the three first plies.

The deconsolidation strain of the samples can then be plotted versus the lower face temperature of the samples (Fig. 13 right). As can be seen from Fig. 13, there is a very good correlation between the final deconsolidation strain obtained with the continuous measurement and with the measurement after experiment, at both measuring points. However, in contrary to analysis after experiment, the sample behavior during heating can be observed thanks to the online and continuous measurement. As shown on Fig. 13, the deconsolidation strain achieved by the sample during the heating is much higher than the final strain.

The sample behavior during heating can be divided in three stages visible in Fig. 13 right.

1. During the first stage, the samples experience thermal expansion as the temperature increases until deconsolidation occurs. A significant slope change is then observed on the deconsolidation strain curve. By observing the evolution of the measured temperature on the sample upper face (TC5), we can also be noted that the deconsolidation onset coincides with a regime change in the sample thermal behavior. This slight drop in temperature can be explained by a decrease in the thermal conductivity of the material due to the appearance of porosities. The temperature measurement can therefore be a mean to detect the deconsolidation onset.
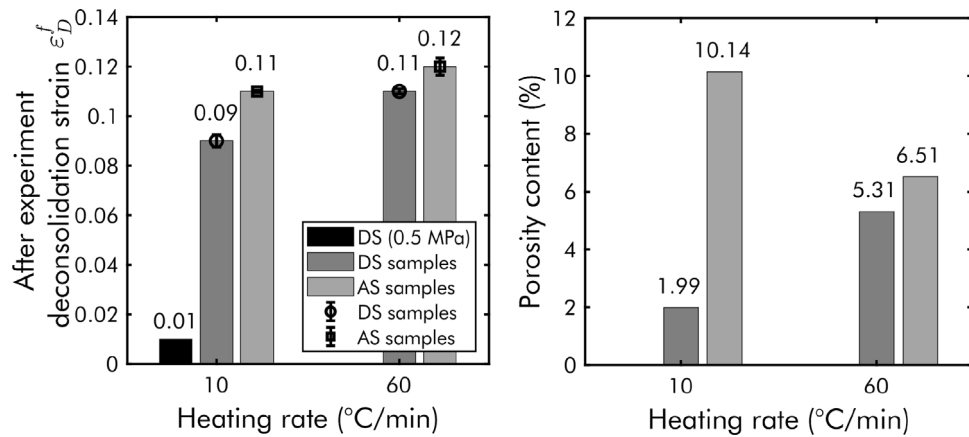
Fig. 11. Data after experiment. (left) deconsolidation strain obtained for each test condition and (right) final porosity content after the experiments.
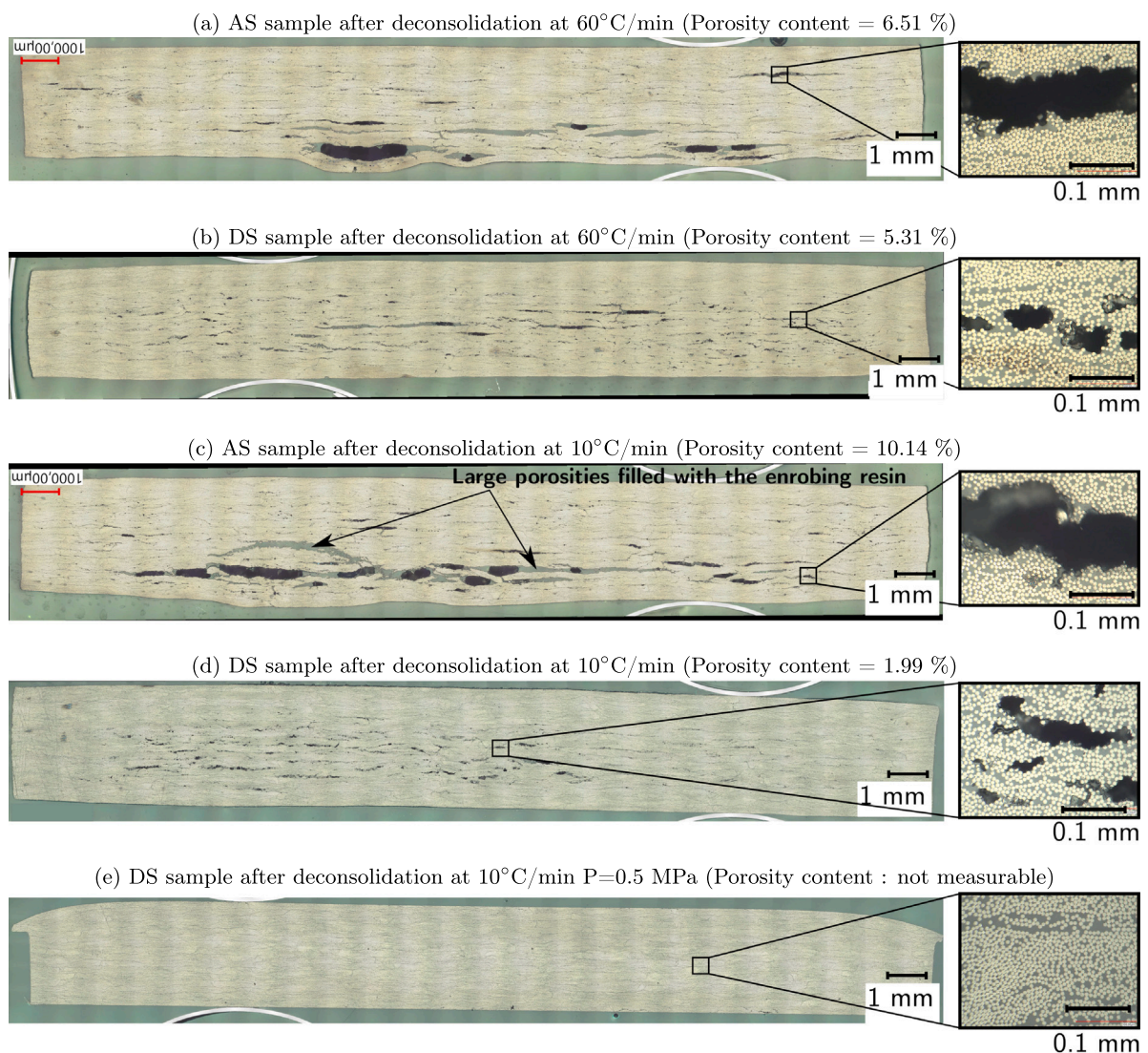

(a) AS sample after deconsolidation at 60°C/min (Porosity content = 6.51 %)

(b) DS sample after deconsolidation at 60°C/min (Porosity content = 5.31 %)

(c) AS sample after deconsolidation at 10°C/min (Porosity content = 10.14 %)

(d) DS sample after deconsolidation at 10°C/min (Porosity content = 1.99 %)

(e) DS sample after deconsolidation at 10°C/min P=0.5 MPa (Porosity content : not measurable)

Fig. 12. Micrographs of deconsolidated samples. After the experiment, the porosities morphology and distribution is very different between AS samples and DS samples.

2. In the second stage, the samples experience deconsolidation which extends during the dwell. During this stage, the deconsolidation strain increases significantly (from $\varepsilon_D = 0.02$ to 0.15) and rapidly ($\dot{\varepsilon}_D \approx 0.64$ s^{-1}).

3. In the last stage, sample shrinkage occurs due to the polymer matrix crystallization and thermal shrinkage during the cooling. During this stage, an increase of the strain, which is a structural artifact related to the sample warpage, may be observed. The
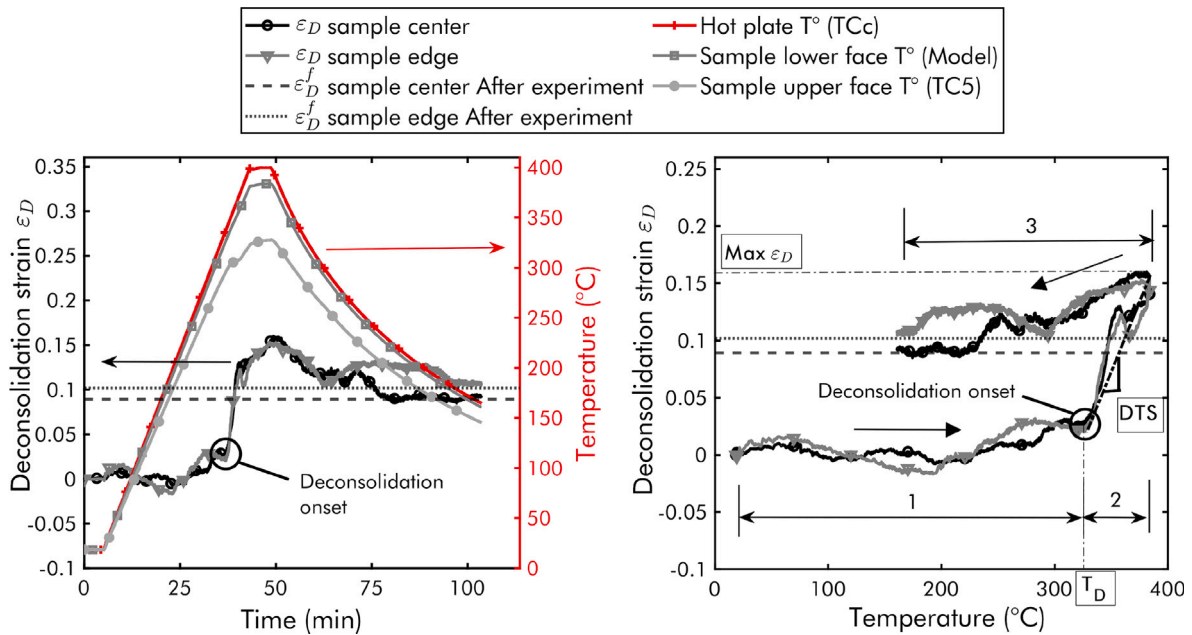
Fig. 13. Continuous and online deconsolidation monitoring. Through thickness deconsolidation strain vs time (left) and deconsolidation strain vs the sample lower face temperature estimated with the thermal model (right) of hot press consolidated sample dried for 72h@180 °C and heated at 10 °C/min without any applied counter pressure.

sample warpage is due to the non uniform temperature field in the sample induced by the unilateral cooling. The warpage effect explains the difference between the final deconsolidation strain obtained by continuous measurement in CODEC and by final thickness measurement. By comparing the curves obtained at the two measurement points, it can be seen that the edge effect is negligible. During the entire heating stage, the maximum difference between the strain obtained at the two measurement points ($\Delta\varepsilon_D$) is 0.02.

Moreover, thanks to this novel online CODEC methodology, several characteristic magnitudes related to the dynamic deconsolidation phenomenon could be quantified (for the first time). These are for instance:

- **Deconsolidation temperature** T_D (°C) characterizes the deconsolidation start. It corresponds to the temperature at which a slope change of the deconsolidation strain curve is observed. Since deconsolidation can start at one point before the other, the final value of deconsolidation temperature retained for the analysis corresponds to the minimum temperature between the two deconsolidation temperatures determined at the two measurement points.
- **Maximum deconsolidation strain** (**Max** ε_D) characterizes the maximal strain induced by deconsolidation during the heating. It corresponds to the maximum deconsolidation strain value achieved by the samples during their heating.
- **Deconsolidation's Thermal Sensitivity DTS** (°C^{-1}) characterizes the sample deconsolidation strain variation with increasing temperature. It is calculated by plotting the sample strain versus the sample lower face temperature (Fig. 13 right). The sample strain values during the deconsolidation stage are then fitted with a linear curve using the least squares method. The DTS corresponds to the linear curve slope value. The maximum DTS, between the two measurement points, was retained for the analysis.
- **Deconsolidation rate** (s^{-1}). Similarly in the deconsolidation versus time plot (Fig. 13 left), a deconsolidation rate can be identified by fitting the strain values during the deconsolidation stage with a linear curve.

4.3. Deconsolidation test results

Fig. 14 shows the measured strains obtained at both heating rates for AS samples and DS samples. First, all the samples experience roughly the same thermal expansion during ramp-up and the same shrinkage during cool down. Second, regardless of the heating rate, two different deconsolidation dynamics are observed. When the sample are initially dried (DS samples), the strain increases smoothly during the ramp-up and even during the dwell. On the opposite, AS samples show a brutal increase of the deconsolidation strain and rather a decrease of the strain during the dwell.

These dynamic structural effects could not have been observed with classical testing after experiment or with standard TMA. Moreover, the maximum deconsolidation strain achieved by AS samples are much higher than DS samples. Finally, no deconsolidation was observed during the test under 0.5 MPa. This pressure is thus high enough to avoid deconsolidation.

From these deconsolidation graphs (Fig. 14), characteristic quantities of deconsolidation were determined (Fig. 15). Under atmospheric pressure (no counter pressure test), deconsolidation appears in the melting zone, but before the material melting peak (338 °C) for both groups of samples at 10 °C/min (Fig. 15 left). At 60 °C/min, the deconsolidation occurs as soon as the temperature reaches the melting zone (310 °C) for AS samples and the melting peak for DS samples. During the deconsolidation stage, independently of the heating rate, the DTS (Fig. 15 middle) and maximum deconsolidation strain (Fig. 15 right) of AS samples are all higher than DS samples. However, in the case of AS samples, the DTS and maximum deconsolidation strain increase with decreasing heating rate while the opposite is observed for DS samples. These observations mean that when the sample is initially dried (DS), a higher heating rate leads to a higher sensitivity of the strain to temperature change (DTS). When moisture is initially present in the sample (AS), a higher heating rate rather leads to a lower sensitivity (DTS). Deconsolidation is thus heating-rate dependent and this dependency is affected by the preconditioning.

Thanks to the online and continuous measurement on CODEC, the large porosities observed in the AS samples can now be explained by the fast and high increase of the porosities size visible on the deconsolidation graphs (Fig. 14). The low porosity content observed
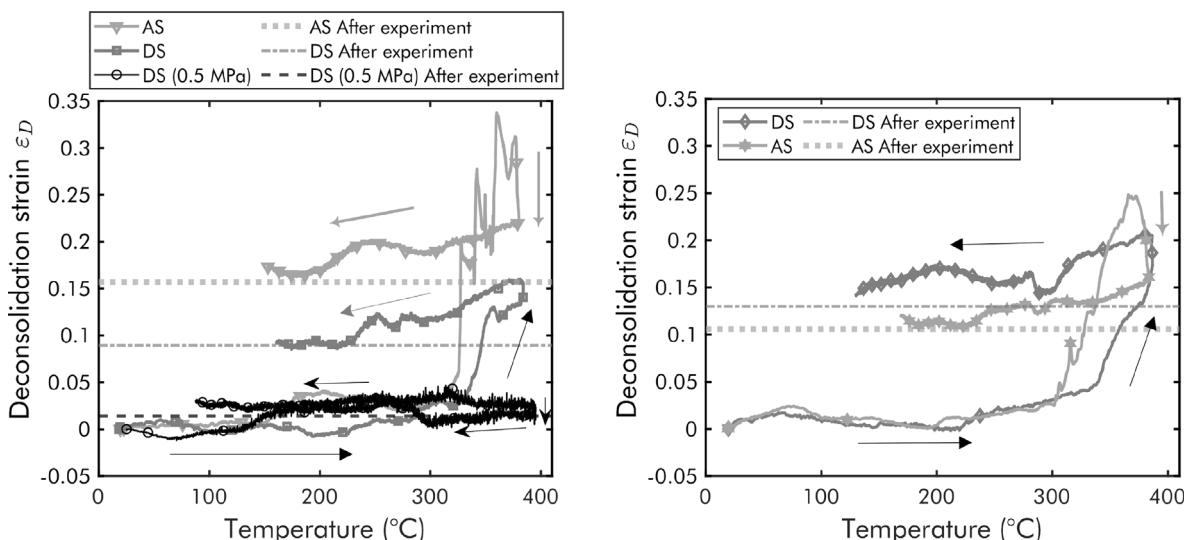
Fig. 14. Deconsolidation graphs obtained at the sample center. Deconsolidation of Dried samples (DS) and Ambient Storage (AS) samples heated at 10 °C/min (left) and at 60 °C/min (right).
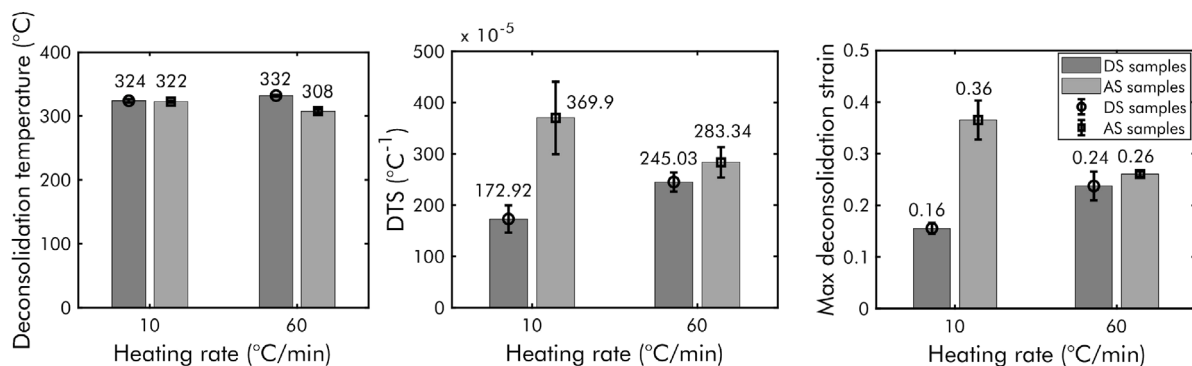

Fig. 15. Effect of moisture and residual stresses on (left) deconsolidation temperature (middle) DTS and (right) maximum deconsolidation strain.

in the DS samples is related to the slow growth of the porosities during the heating, also visible in the deconsolidation graphs. Hence, the sample behavior during heating described by the online measurements correlates with the sample final microstructure. This correlation shows that the porosity final morphologies and distribution are highly affected by the dynamic mechanisms during the sample heating. Therefore, the online measurements on the CODEC device provide a better understanding of the mechanisms involved during deconsolidation.

4.4. Discussion

There was initially no moisture in DS samples. It is assumed that there are also no residual volatiles from additives such as plasticizers. Indeed, the additives used in TPC prepreg manufacturing, often have a higher boiling point (≫100 °C) compared to water. However, their boiling point are lower than the melting temperature of the high performance polymer matrix. In our case where the laminates have been pre-consolidated, most additives evaporated during the initial laminate consolidation process. For example, after consolidation in press of CF/PEEK laminates, Slange et al. [13] did not detect any residual volatiles (from additives) other than water with residual gas analysis (RGA). The DS sample deconsolidations are thus attributed to the residual stresses effect. During consolidation, residual stresses are trapped in the laminates during cooling. For hot press consolidation, the cooling was done at 10 °C/min under a pressure of 4 MPa. Therefore, in addition to fiber bed compaction stresses, stresses due to thermal and crystallization shrinkage, and eventually the skin-core

thermal gradient are not fully relaxed before the material solidification. During deconsolidation tests, when the temperature reaches T_m, the residual stresses trapped in the matrix and the fibrous network can relax. This causes the formation of porosities in the matrix and at the fiber–matrix interfaces through complex local relaxation phenomena. When the applied counter pressure is greater than the internal stress, deconsolidation does not occur. This is the case for the test with a high counter pressure. Thus, the application of a counter pressure of 0.5 MPa is sufficient to limit the amplitude of deconsolidation, hence the decrease of the DTS and the maximum deconsolidation strain.

Varying the heating rate gives insight on the effect of moisture or residual stresses. In the case of DS samples, an increase in heating rate leads to an increase in deconsolidation strain (see Fig. 15). We assume that in addition to the higher thermal gradient through thickness, the composite material does not have enough time to relax residual stresses before melting. On the contrary, in the case of AS samples, an increase in heating rate results in a decrease in deconsolidation. This cannot be attributed to residual stress effects. We assume that this is rather dissolved moisture which cannot diffuse and coalesce at high heating rate. Thus, the presence of moisture is also involved in deconsolidation.

This is also supported by the micrographs. The porosities in AS samples are mainly located at the samples subsurface (see Fig. 12 a & c). We believe these porosities are the consequence of moisture. The initial porosities nucleate in the vicinity of the hot plate. Once formed, the remaining moisture from the laminate may diffuse in these voids. In the case of DS samples (see Fig. 12 b & d), there is smaller porosities

located in the center. It suggests that the drying has not been effective down to the core of the laminate.

These are, to our knowledge, the first deconsolidation experiments using online measurements in representative conditions of TPC laminates processing. Residual stresses and moisture trapped in the preconsolidated laminates are driving deconsolidation. These conclusions could not have been reached with an after experiment measurement only.

5. Conclusion

The phenomenon of deconsolidation is a major problem that limits the application of thermoplastic composites in aeronautics structures. In spite of the research carried out on this subject in the literature, several questions on the causes of deconsolidation are still unanswered. The generally used means of deconsolidation characterization do not allow investigation into what happens during deconsolidation under representative process conditions.

For this reason, a new TMA device called CODEC has been developed in this study. The device allows to characterize the deconsolidation continuously and online, on large samples (up to 150 mm × 50 mm), under industrial conditions. The deconsolidation characterization on CODEC is performed by contactless thickness variation measurement with a relative error of ±2%. This novel bench allows for a temperature and pressure control reproducing industrial manufacturing conditions. Hence, CODEC allows tracking of the deconsolidation kinetics during processing.

The CODEC device was used to investigate the effect of residual stresses, moisture, and heating rate, during the re-heating stage of a pre-consolidated laminate. The deconsolidation tests were performed on UD laminate samples consolidated in a hot press. Some samples were thoroughly dried to eliminate possible effects of moisture content and others were stored in ambient condition.

Thanks to the online and continuous measurement on CODEC device, the effect of moisture and residual stresses were highlighted. Contrary to what is mainly found in the literature, the effect of residual stresses is not negligible. The measurements on CODEC also showed an effect of the heating rate on the deconsolidation phenomenon. From the different behavior obtained at the different heating rates, two main mechanisms appear to be involved in deconsolidation: stress relaxation, moisture diffusion and coalescence. Finally, the deconsolidation kinetics measured correlates with the final porosities content and morphologies observed on micrographs after experiment.

Nevertheless, it should be noted that these results do not show the leading mechanism of deconsolidation. Do porosities grow mainly by moisture diffusion and coalescence or by stress relaxation? What is the contribution of moisture or residual stresses during deconsolidation? Furthermore, all the tests performed in this study were performed on UD laminates. Do these observations remain valid for other ply stacking sequences? In order to answer these questions, further investigations are needed to have a better understanding of deconsolidation which is now made possible thanks to the CODEC device. These questions will be the subject of further investigations.

CRediT authorship contribution statement

Luc Amedewovo: Methodology, Validation, Formal analysis, Investigation, Writing, Visualization. **Arthur Levy:** Conceptualization, Methodology, Formal analysis, Investigation, Writing – review & editing, Supervision. **Basile de Parscau du Plessix:** Formal analysis, Ressource, Supervision, Funding acquisition, Project administration. **Julien Aubril:** Software. **Arnaud Arrive:** Ressources. **Laurent Orgéas:** Conceptualization, Methodology, Supervision. **Steven Le Corre:** Conceptualization, Methodology, Formal analysis, Supervision, Project administration, Funding acquisition.

Declaration of competing interest

Data availability

Data will be made available on request.

Acknowledgments

References

[1] Sarr Cheikh, Chataigner Sylvain, Gaillet Laurent, Godin Nathalie. Auscultation des assemblages collés par acousto-ultrasons : Application à des assemblages acier-composite du génie civil. J Natl sur Les Composites 2019.

[2] Robles Julieta Barroeta, Cole Richard, Sands James M. Development of controlled adhesive bond strength for assessment by advanced non-destructive inspection techniques. Soc Adv Mater Process Eng 2010.

[3] Crane Robert Lee, Dillingham Giles. Composite bond inspection. J Mater Sci 2008;43:6682–94.

[4] Shi H, Villegas I Fernandez, Bersee HEN. Strength and failure modes in resistance welded thermoplastic composite joints: Effect of fibre-matrix adhesion and fibre orientation. Composites A 2013;55:1–10.

[5] Hagstrand PO, Bonjour F, Månson JAE. The influence of void content on the structural flexural performance of unidirectional glass fibre reinforced polypropylene composites. Composites A 2005;36:705–14.

[6] Liu Xueshu, Chen Fei. A review of void formation and its effects on the mechanical performance of carbon fiber reinforced plastic. Eng Trans 2016;64:33–51.

[7] Grunenfelder LK, Nutt SR. Void formation in composite prepregs - Effect of dissolved moisture. Compos Sci Technol 2010;70:2304–9.

[8] Anderson J, Altan M. Formation of voids in composite laminates: Coupled effect of moisture content and processing pressure. Polym Compos 2014.

[9] de Parscau du Plessix Basile. Analyse et modélisation du développement de porosités lors de la cuisson de pièces composites thermodurcissables hautes performances [Ph.D. thesis], Université de Nantes; 2016.

[10] Leterrier Y, G'sell C. Formation and elimination of voids during the processing of thermoplastic matrix composites. Polym Compos 1994;15:101–5.

[11] Roychowdhury S, Gillespie JW, Advani SG. Volatile-induced void formation in amorphous thermoplastic polymeric materials: I. Modeling and parametric studies. J Compos Mater 2001;35:340–66.

[12] Shi Huajie, Villegas Irene Fernandez, Bersee Harald EN. Analysis of void formation in thermoplastic composites during resistance welding. J Thermoplast Compos Mater 2017;30:1654–74.

[13] Slange TK, Warnet LL, Grouve WJB, Akkerman R. Deconsolidation of C/PEEK blanks: On the role of prepreg, blank manufacturing method and conditioning. Composites A 2018;113:189–99.

[14] Lu Meng, Ye Lin, Mai Yiu Wing. Thermal de-consolidation of thermoplastic matrix composites-II. "Migration" of voids and "re-consolidation". Compos Sci Technol 2004;64:191–202.

[15] Ye Lin, Chen Zuo Rong, Lu Meng, Hou Meng. De-consolidation and re-consolidation in CF/PPS thermoplastic matrix composites. Composites A 2005;36:915–22.

[16] Wolfrath J, Michaud V, Månson JAE. Deconsolidation in glass mat thermoplastic composites: Analysis of the mechanisms. Composites A 2005;36:1608–16.

[17] Donadei Valentina, Lionetto Francesca, Wielandt Michael, Offringa Arnt, Maffezzoli Alfonso. Effects of blank quality on press-formed PEKK/Carbon composite parts. Materials 2018;11.

[18] Brzeski Markus, Mitschang Peter. Deconsolidation and its interdependent mechanisms of fibre reinforced polypropylene. Polym Polym Compos 2015;23:515–24.

[19] Slange Tjitse Kay. Rapid manufacturing of tailored thermoplastic composites by automated lay-up and stamp forming [Ph.D. thesis], University of Twente; 2019.

[20] Brzeski Markus. Experimental and analytical investigation of deconsolidation for fiber reinforced thermoplastic composites [Ph.D. thesis], TU Kaiserslautern; 2014.

[21] Perez-Martin Helena, Mackenzie Paul, Baidak Alex, Brádaigh Conchúr MÓ, Ray Dipa. Crystallinity studies of PEKK and carbon fibre/PEKK composites: A review. Composites B 2021;223:109127.

[22] Avenet Julien. Assemblage par fusion de composites à matrice thermoplastique: Caractérisation expérimentale et modélisation de la cinétique d'auto-adhésion hors équilibre [Ph.D. thesis], Université de Nantes (UN); 2021.

[23] Pérez-Martín Helena, Mackenzie Paul, Baidak Alex, Brádaigh Conchúr MÓ, Ray Dipa. Crystallisation behaviour and morphological studies of PEKK and carbon fibre/PEKK composites. Composites A 2022;106992.

[24] Arganda-Carreras Ignacio, Kaynig Verena, Rueden Curtis, Eliceiri Kevin W, Schindelin Johannes, Cardona Albert, et al. Trainable Weka segmentation: A machine learning tool for microscopy pixel classification. Bioinformatics 2017;33:2424–6.

[25] Paganin David, Mayo Sheridan C, Gureyev Tim E, Miller Peter R, Wilkins Steve W. Simultaneous phase and amplitude extraction from a single defocused image of a homogeneous object. J Microsc 2002;206(1):33–40.

[26] Lepoivre Arthur. Étude des transferts thermiques et de l'adhésion à l'échelle du cordon dans le procédé de fabrication additive FFF (extrusion de filament fondu) [Ph.D. thesis], Université de Nantes (UN); 2021.

[27] COMSOL Multiphysics® v.6.0.. 2022, COMSOL AB, Stockholm, Sweden, URL https://www.comsol.com.

[28] MATLAB (R2022a). 2022.